AGU PUBLICATIONS

JGR

Journal of Geophysical Research: Atmospheres

RESEARCH ARTICLE
10.1002/2014JD021814

Key Points:
- Turbulent flux estimation with dual-source variational data assimilation scheme
- Models are developed to study the land-atmosphere interaction
- Land surface temperature is retrieved from GOES

Correspondence to:
T. Xu,
xutr@bnu.edu.cn

Citation:
Xu, T., S. M. Bateni, S. Liang, D. Entekhabi, and K. Mao (2014), Estimation of surface turbulent heat fluxes via variational assimilation of sequences of land surface temperatures from Geostationary Operational Environmental Satellites, *J. Geophys. Res. Atmos.*, *119*, 10,780–10,798, doi:10.1002/2014JD021814.

Received 25 MAR 2014
Accepted 31 AUG 2014
Accepted article online 4 SEP 2014
Published online 27 SEP 2014

Estimation of surface turbulent heat fluxes via variational assimilation of sequences of land surface temperatures from Geostationary Operational Environmental Satellites

Tongren Xu[1], S. M. Bateni[2], S. Liang[3,4], D. Entekhabi[5], and Kebiao Mao[6]

[1]State Key Laboratory of Remote Sensing Science, Research Center for Remote Sensing and GIS and School of Geography, Beijing Normal University, Beijing, China, [2]Department of Civil and Environmental Engineering and Water Resource Research Center, University of Hawaii at Manoa, Honolulu, Hawaii, USA, [3]State Key Laboratory of Remote Sensing Science and College of Global Change and Earth System Science, Beijing Normal University, Beijing, China, [4]Department of Geographical Sciences, University of Maryland, College Park, Maryland, USA, [5]Department of Civil and Environmental Engineering, Massachusetts Institute of Technology, Cambridge, Massachusetts, USA, [6]National Hulunber Grassland Ecosystem Observation and Research Station, Institute of Agricultural Resources and Regional Planning, Chinese Academy of Agricultural Sciences, Beijing, China

Abstract Recently, a number of studies have focused on estimating surface turbulent heat fluxes via assimilation of sequences of land surface temperature (LST) observations into variational data assimilation (VDA) schemes. Using the full heat diffusion equation as a constraint, the surface energy balance equation can be solved via assimilation of sequences of LST within a VDA framework. However, the VDA methods have been tested only in limited field sites that span only a few climate and land use types. Hence, in this study, combined-source (CS) and dual-source (DS) VDA schemes are tested extensively over six FluxNet sites with different vegetation covers (grassland, cropland, and forest) and climate conditions. The CS model groups the soil and canopy together as a single source and does not consider their different contributions to the total turbulent heat fluxes, while the DS model considers them to be different sources. LST data retrieved from the Geostationary Operational Environmental Satellites are assimilated into these two VDA schemes. Sensible and latent heat flux estimates from the CS and DS models are compared with the corresponding measurements from flux tower stations. The results indicate that the performance of both models at dry, lightly vegetated sites is better than that at wet, densely vegetated sites. Additionally, the DS model outperforms the CS model at all sites, implying that the DS scheme is more reliable and can characterize the underlying physics of the problem better.

1. Introduction

Sensible and latent heat fluxes are the key variables in energy and water vapor exchange between the land surface and the atmosphere. Latent heat flux is the coupling link between the surface water, energy, and carbon exchanges with the atmosphere. Several techniques (e.g., lysimeters, eddy covariance systems, Bowen ratio methods, and large-aperture scintillometers) have been used to measure surface heat fluxes [*Liu et al.*, 2011, 2013]. However, in situ measurements of heat fluxes are costly and are therefore distributed sparsely and cover only limited time periods. Consequently, a number of models have been developed to estimate surface heat fluxes from remotely sensed land surface temperature (LST) observations.

LST lies at the heart of the surface energy balance (SEB) equation. All components of the SEB equation (i.e., sensible, latent, and ground heat fluxes as well as net radiation) are related to LST. Recently, *Bateni and Entekhabi* [2012a] showed that LST observations contain implicit information on the partitioning of available energy among the SEB components. LST observations have been utilized in three main groups of studies to estimate surface heat fluxes. The first group of studies is diagnostic. These studies use LST to solve the SEB equation and retrieve surface energy fluxes [*Norman et al.*, 1995; *Anderson et al.*, 1997; *Bastiaanssen et al.*, 1998a, 1998b; *Su*, 2002; *Liu et al.*, 2007a; *Jia et al.*, 2009; *Ma et al.*, 2012]. In this group, the ground heat flux is usually taken as an empirical fraction of the net radiation. Additionally, surface heat fluxes can be retrieved only for instances in which remotely sensed LSTs are available. The second group is known as triangle

approaches; these studies attempt to estimate the surface evaporation using empirical relationships between LST and vegetation indices such as the normalized difference vegetation index and leaf area index (LAI) [*Jiang and Islam*, 2001, 2003; *Nishida et al*., 2003; *Wang et al*., 2006; *Tang et al*., 2010; *Sun et al*., 2013]. These methods need to define the dry and wet edges of the triangle space, which is site specific.

The third group of studies estimates the surface heat fluxes by assimilating sequences of LST measurements within a variational data assimilation (VDA) framework using the parsimonious force-restore equation as a constraint [*Castelli et al*., 1999; *Boni et al*., 2001; *Caparrini et al*., 2003, 2004a, 2004b; *Crow and Kustas*, 2005; *Qin et al*., 2007; *Sini et al*., 2008]. In contrast to the diagnostic and triangle approaches, this group of methods does not require any empirical or site-specific relationships and can provide temporally continuous surface heat flux estimates from discrete spaceborne LST observations.

The VDA utilizes combined-source (CS) and dual-source (DS) schemes to simulate interaction between the land surface and the overlying air and to retrieve surface heat fluxes. The CS scheme does not distinguish the difference between soil and canopy temperatures and treats LST as the effective temperature of a mixed soil-vegetation medium. In contrast, the DS scheme accounts for the difference between soil and canopy temperatures and considers the interactions of the soil and canopy with the overlying atmosphere separately.

Bateni and Liang [2012] and *Bateni et al*. [2013a, 2013b] significantly advanced the CS and DS VDA approaches by using the full heat diffusion equation as a physical constraint instead of the simple force-restore equation. However, the *Bateni and Liang* [2012] and *Bateni et al*. [2013a, 2013b] CS and DS VDA approaches have been tested so far only at two humid sites with grassland vegetation cover (the First International Field Experiment and the Southern Great Plains sites). In this study, the performance of the recently augmented CS and DS VDA frameworks is assessed in detail using surface heat fluxes collected at six FluxNet sites. These sites are chosen such that they sample different climatic and vegetative conditions in an effort to evaluate the robustness of the VDA schemes in various hydrological environments.

Sequences of daytime LST observations have various diurnal amplitudes depending on the available energy and the relative efficiency of SEB components [*Bateni and Entekhabi*, 2012a]. Hence, an accurate characterization of the LST diurnal cycle is of vital importance for the reliable performance of the VDA methods. In this study, LST data from Geostationary Operational Environmental Satellites (GOES) are assimilated in the CS and DS VDA schemes to estimate surface heat fluxes. GOES can accurately characterize the LST diurnal cycle by providing LST data every 30 min and thus can significantly advance the robustness of the VDA framework. GOES LST can be accurately retrieved [*Sun et al*., 2004] and proved to be a significant data set for improving turbulent flux estimates of land surface model [*Xu et al*., 2011].

This paper is organized as follows. Section 2 introduces methodology, including heat diffusion equation, surface energy balance equations, and adjoint state formulation. Section 3 presents the six FluxNet sites at which the CS and DS VDA systems are tested along with the LST retrieved from GOES. Section 4 shows the results and discussions. Sensitivity analyses are given in section 5. Finally, conclusions are reported in section 6.

2. Methodology

The CS and DS VDA schemes, which were developed by *Bateni and Liang* [2012] and *Bateni et al*. [2013a], are used in this study. They are summarized hereinafter. The heat diffusion equation (which models the soil temperature dynamics) along with its boundary conditions are described in section 2.1, the CS and DS SEB schemes are presented in section 2.2, and the adjoint state formulation and the Euler–Lagrange equations are shown in section 2.3.

2.1. Heat Diffusion Equation

The soil temperature at depth z and time t, $T(z,t)$, is given by the heat diffusion equation, which is given by

$$C\frac{\partial T(z,t)}{\partial t} = P\frac{\partial T^2(z,t)}{\partial z^2} \tag{1}$$

where C and P are, respectively, the soil volumetric heat capacity ($\mathrm{J\,m^{-3}\,K^{-1}}$) and thermal conductivity ($\mathrm{W\,m^{-1}\,K^{-1}}$). For simplicity, in this paper, $T(z=0,t)$ is indicated by $T(t)$.

The boundary conditions at the top and bottom of the soil column are required to solve the heat diffusion equation. The boundary condition at the top of the soil column, $T(z=0,t)$, is retrieved from the surface boundary forcing equation $-PdT(z=0,t)/dz = G(t)$ (where $G(t)$ is the ground heat flux at time t) [*Bateni et al.*, 2013a]. At the bottom boundary, a Neumann boundary condition is implemented as

$$dT(l,t)/dz = 0 \tag{2}$$

where l is the depth of the bottom boundary condition, which is set to 0.5 m [*Hu and Islam*, 1995; *Bateni and Liang*, 2012; *Bateni et al.*, 2013a]. The heat diffusion equation is solved using an implicit finite difference scheme. The detailed information on discretization of the heat diffusion equation and its numerical implementation can be found in *Bateni et al.* [2012].

2.2. Surface Energy Balance (SEB)

The CS SEB scheme considers the soil and vegetation as a single source and follows that of *Bateni et al.* [2013a]. For the CS approach, the land surface energy balance equation can be written as

$$G = R_N - H - LE \tag{3}$$

where G is the ground heat flux (W m^{-2}), H and LE are the sensible and latent heat fluxes (W m^{-2}), and R_N is the net radiation (W m^{-2}) that is obtained according to *Bateni et al.* [2013a].

The sensible heat flux can be obtained with the LST (T) generated by the heat diffusion equation as follows:

$$H = \rho c_p C_H U(T - T_A) \tag{4}$$

where ρ is the air density (kg m^{-3}), c_p is the heat capacity of air (1012 J kg^{-1} K^{-1}), U and T_A are, respectively, the wind speed (m s^{-1}) and air temperature (K) at a reference height, and C_H is the bulk heat transfer coefficient (-). The bulk heat transfer coefficient (C_H) can be written as the product of the neutral bulk heat transfer coefficient (C_{HN}) and a correction function for atmospheric stability, $f(Ri)$ (i.e., $C_H = C_{HN} f(Ri)$, where Ri is the Richardson number). C_{HN} can be related to roughness length scales for heat and momentum [*Liu et al.*, 2007b; *Zhang et al.*, 2010], which is mainly a function of vegetation phenology and is assumed to vary on a monthly temporal scale [*McNaughton and Van den Hurk*, 1995; *Jensen and Hummelshøj*, 1995; *Qualls and Brutsaert*, 1996; *Crow and Kustas*, 2005; *Bateni et al.*, 2013b]. It scales the sum of turbulent heat fluxes ($H + LE$) and constitutes the first unknown parameter of the CS scheme. Following *Crow and Kustas* [2005], *Sini et al.* [2008], *Bateni and Liang* [2012], and *Bateni and Entekhabi* [2012b], the atmospheric correction function (f) proposed by *Caparrini et al.* [2003] is used herein.

The second unknown of the CS scheme is evaporative fraction (EF), which scales partitioning between the turbulent heat fluxes and is given by

$$\mathrm{EF} = LE/(H + LE) \tag{5}$$

The DS SEB scheme developed by *Bateni and Liang* [2012] is used in this study. The DS can model interaction within the soil-canopy-atmosphere system [*Kustas et al.*, 1996; *Bateni and Liang*, 2012]. In the DS SEB model, the net radiation absorbed by the canopy (R_{NC}) is partitioned between the sensible (H_C) and latent (LE_C) heat fluxes for the canopy ($R_{NC} = H_C + LE_C$, the subscript "C" refers to the vegetation canopy). The ground heat flux (G) can be calculated as the residual of the surface energy balance for soil [*Bateni and Liang*, 2012].

The sensible heat fluxes for the canopy (H_C) and soil (H_S) can be estimated via [*Bateni and Liang*, 2012]

$$H_C = \rho c_p C_{HC} U_W (T_C - T_W) \tag{6a}$$

$$H_S = \rho c_p C_{HS} U_W (T_S - T_W) \tag{6b}$$

where U_W and T_W are, respectively, the wind speed and air temperature at a reference height within the canopy, T_C and T_S are the canopy and soil temperatures, and C_{HC} and C_{HS} are the bulk heat transfer coefficients from leaves and soil to air within the canopy (-). T_S is estimated with the heat diffusion equation (equation (1)). Equations for the estimation of T_C and T_W can be found in *Bateni and Liang* [2012]. C_{HC} and C_{HS} are related to C_{HN} to decrease the number of unknown parameters of the DS scheme. For detailed information, the reader is referred to *Bateni and Liang* [2012] and *Bateni et al.* [2013b].

The total sensible heat flux (H) can be estimated via

$$H = \rho c_p C_H U (T_W - T_A) \tag{7}$$

Similar to the CS SEB scheme, C_H is related to C_{HN} (the unknown of the model) via $C_H = C_{HN} f(Ri)$. The total sensible heat flux (H) is also given by the weighted average of sensible heat fluxes from the canopy and soil:

$$H = f_C H_C + (1 - f_C) H_S \tag{8}$$

where f_C is the vegetation cover fraction. The evaporative fractions for the soil and canopy (EF_S and EF_C) are the other unknown parameters of the DS scheme and are given by

$$EF_C = LE_C/(H_C + LE_C) \tag{9a}$$

$$EF_S = LE_S/(H_S + LE_S) \tag{9b}$$

C_{HN}, EF_C, and EF_S are the three unknown parameters of the DS SEB scheme that are estimated via a VDA framework.

In the DS SEB scheme, the effective LST is calculated through a composite of the soil and canopy temperatures as follows:

$$T = \left[f_C T_C^4 + (1 - f_C) T_S^4\right]^{0.25} \tag{10}$$

2.3. Adjoint State Formulation

As mentioned in section 2.2, C_{HN} and EF constitute the unknown parameters of the CS SEB scheme that should be estimated by the VDA approach. In the DS SEB model, three unknown parameters, namely, C_{HN}, EF_C, and EF_S, must be estimated. C_{HN} varies on a monthly time scale (i.e., the scale of vegetation phenology), and thus, one C_{HN} value is retrieved in each monthly modeling period [*Caparrini et al.*, 2003, 2004a, 2004b; *Crow and Kustas*, 2005; *Bateni and Liang*, 2012; *Bateni and Entekhabi*, 2012b; *Bateni et al.*, 2013a, 2013b]. EF is self preserved during daytime hours (i.e., 09:00–16:00 LT), but it can vary from day to day [*Gentine et al.*, 2007].

A cost function (J) is defined to retrieve the unknown parameters of the CS scheme (i.e., C_{HN} and EF) by minimizing the difference between the LST observations (from GOES) and estimates (from the heat diffusion equation). The cost function for the CS model can be written as

$$\begin{aligned} J(T, R, \mathrm{EF}, \lambda) = &\sum_{i=1}^{N} \int_{t_0}^{t_1} \left[T_{obs,i}(t) - T_i(t)\right]^T K_T^{-1} \left[T_{obs,i}(t) - T_i(t)\right] dt + \left(R - R'\right)^T K_R^{-1} \left(R - R'\right) \\ &+ \sum_{i=1}^{N} \left(\mathrm{EF}_i - \mathrm{EF}_i'\right)^T K_{\mathrm{EF}}^{-1} \left(\mathrm{EF}_i - \mathrm{EF}_i'\right) + 2 \sum_{i=1}^{N} \int_{t_0}^{t_1} \int_0^l \lambda_i(z,t) \left[\frac{\partial T_i(z,t)}{\partial t} - D \frac{\partial^2 T_i(z,t)}{\partial z^2}\right] dz dt z \end{aligned} \tag{11}$$

The first term on the right-hand side measures the difference between the GOES-measured LST (T_{obs}) and the predicted LST (T). C_{HN} is transformed to R via $C_{HN} = \exp(R)$ to make it strictly positive and meaningful. The second and third terms measure the difference between the parameter estimates (R and EF) and their prior values (R' and EF'). As mentioned before, C_{HN} is hypothesized to be constant over the entire monthly assimilation period ($N = 30$ days), and EF is postulated to be invariant over each day during the assimilation window (i.e., from $t_0 = 9{:}00$ to $t_1 = 16{:}00$ LT). The last term is the heat diffusion equation, which is adjoined to the model (as a physical constraint) via the Lagrange multiplier, λ. $D = P/C$ is the heat diffusion coefficient. K_T^{-1}, K_R^{-1}, and K_{EF}^{-1} are the numerical constant parameters that weigh each term in the objective function and control its rate of convergence. Following *Bateni et al.* [2013a], K_T^{-1}, K_R^{-1}, and K_{EF}^{-1} are set to 0.01 K^{-2}, 1000, and 1000, respectively.

The optimal values for C_{HN} and EF are found by minimizing the cost function. To minimize the cost function, its first variation should be set to zero ($\Delta J = 0$) [*Bennett*, 2002]. Setting ΔJ to zero leads to a number of Euler–Lagrange equations that should be solved simultaneously through an iterative loop to obtain optimal values of C_{HN} and EF. The Euler–Lagrange equations for the CS VDA scheme can be found in *Bateni et al.* [2013a].

Similarly, C_{HN}, EF_S, and EF_C are estimated by minimizing the difference between the GOES LST and the effective LST estimates (equation (10)). The cost function for the DS model is defined as

$$J(T,R,EF_S,EF_C,\lambda)=\sum_{i=1}^{N}\int_{t_0}^{t_1}\left[T_{obs,i}(t)-T_i(t)\right]^T K_T^{-1}\left[T_{obs,i}(t)-T_i(t)\right]dt+\left(R-R'\right)^T K_R^{-1}\left(R-R'\right)$$
$$+\sum_{i=1}^{N}\left(EF_{S,i}-EF'_{S,i}\right)^T K_{EF_S}^{-1}\left(EF_{S,i}-EF'_{S,i}\right)+\sum_{i=1}^{N}\left(EF_{C,i}-EF'_{C,i}\right)^T K_{EF_C}^{-1}\left(EF_{C,i}-EF'_{C,i}\right)$$
$$+2\sum_{i=1}^{N}\int_{t0}^{t1}\int_0^l\lambda_i(z,t)\left[\frac{\partial T_{S,i}(z,t)}{\partial t}-D\frac{\partial T_{S,i}^2(z,t)}{\partial z^2}\right]dzdt \tag{12}$$

where the third and fourth terms on the right-hand side of equation (12) measure the difference between the soil and canopy evaporative fraction estimates and their prior values, respectively. K_T^{-1}, K_R^{-1}, $K_{EF_S}^{-1}$, and $K_{EF_C}^{-1}$ are, respectively, set to 0.01 K^{-2}, 1000, 1000, and 1000 based on *Bateni and Liang* [2012].

In the DS VDA scheme, the optimal values for C_{HN}, EF_S, and EF_C are found by minimizing the cost function (equation (12)). Setting ΔJ to zero yields a number of Euler–Lagrange equations as follows:

$$\frac{\partial\lambda}{\partial t}+D\frac{\partial^2\lambda}{\partial z^2}=0 \tag{13a}$$

$$\lambda(z,t_1)=0 \tag{13b}$$

$$\left.\frac{\partial\lambda}{\partial z}\right|_{z=0}=\frac{K_T^{-1}}{D}(T-T_{obs})(1-f_C)T_S^3T^{-3}+\frac{\lambda(0,t)}{P}\left[4\varepsilon_S\sigma T_S^3+\frac{\rho c_P e^R f\,(Ri)U\exp(-LAI)}{1-EF_S}\right](1-f_C) \tag{13c}$$

$$\left.\frac{\partial\lambda}{\partial z}\right|_{z=l}=0 \tag{13d}$$

$$R=R'-\frac{1}{C\bullet K_R^{-1}}\sum_{i=1}^{N}\int_{t0}^{t1}\lambda_i(0,t)\left[\frac{\rho c_P e^R f\,(Ri)U\exp(-LAI)(T_S-T_W)}{1-EF_{S,i}}\right](1-f_C)dt$$
$$-\frac{K_T^{-1}}{K_R^{-1}}\sum_{i=1}^{N}\int_{t0}^{t1}(T-T_{obs})\frac{\rho c_P e^R f\,(Ri)U\exp(-0.5\ LAI)(T_W AA-BB)}{AA^2}f_C T_C^3T^{-3}dt \tag{14a}$$

$$EF_{S,i}=EF'_{S,i}-\frac{1}{C\bullet K_{EF_S}^{-1}}\int_{t0}^{t1}\frac{\lambda(0,t)}{\left(1-EF_{S,i}\right)^2}\rho c_P e^R f\,(Ri)U\exp(-LAI)(T_S-T_W)(1-f_C)dt \tag{14b}$$

$$EF_{C,i}=EF'_{C,i}-\frac{K_R^{-1}}{K_{EF_C}^{-1}}\int_{t0}^{t1}\frac{4\varepsilon_S\sigma T_A^3BB-\left[(1-\alpha_C)R_S^{\downarrow}+R_L^{\downarrow}+3\,\varepsilon_S\sigma T_A^4\right]AA}{AA^2}f_C T_C^3T^{-3}(T-T_{obs}) \tag{14c}$$

where $AA=4\,\varepsilon_S\sigma T_A^3(1-EF_C)+\rho c_P C_{HN}f(Ri)\exp(-0.5\ LAI)U$, $BB=\left[(1-\alpha_C)R_S^{\downarrow}+R_L^{\downarrow}+3\varepsilon_S\sigma T_A^4\right](1-EF_C)+\rho c_P C_{HN}f(Ri)\exp(-0.5\ LAI)UT_W$, ε_S is the soil emissivity (-), σ is the Stefan–Boltzmann constant ($5.67\times10^{-8}\,W\,m^{-2}\,K^{-4}$), and $R_S^{\downarrow}$ and $R_L^{\downarrow}$ are the downward shortwave and longwave radiation ($W\,m^{-2}$).

The adjoint model (equation (13a)) has to be integrated backward in time using the terminal and boundary conditions (equations (13b), (13c), and (13d)). The unknown parameters of the DS scheme (i.e., R, EF_S, and EF_C) can be estimated via equations (14a), (14b), and (14c). The DS VDA scheme improves the estimates of the three unknown parameters iteratively starting from the initial guesses (R', EF_S', and EF_C').

3. Data Sets

Surface heat flux measurements from six AmeriFlux sites (http://public.ornl.gov/ameriflux) (which sample a fairly wide range of hydrological and vegetative conditions) are used to evaluate the performance of the CS and DS models. These sites and their vegetative and soil moisture conditions are listed in Table 1. Their locations are shown in Figure 1. The experimental sites include three types of vegetation cover: grassland, cropland, and forest. LAI varies over a wide range of values across the experimental sites, from 1.6 (at a sparsely vegetated site) to 5.4 (at a densely vegetated site). Soil moisture (SM) also ranges from 0.19 (at a dry site) to 0.43 (at a wet site). The wide range of soil moisture and LAI values allows us to assess the robustness of the CS and DS VDA models under different environmental conditions, because these two

Table 1. Summary of the Characteristics Over Six Study Sites[a]

Site	Location	Land Cover	LAI ($m^2 m^{-2}$)	f_C	SM ($m^3 m^{-3}$)	C ($J m^{-3} K^{-1}$)	P ($J m^{-1} K^{-1} s^{-1}$)
Brookings	44.34°N, 96.83°W	Grassland	1.6	0.55	0.43	3.04×10^6	1.64
Goodwin	34.25°N, 89.97°W	Grassland	1.8	0.59	0.31	2.57×10^6	1.75
Bondville	40.01°N, 88.29°W	Cropland	2.7	0.74	0.32	2.58×10^6	1.55
Mead	41.16°N, 96.47°W	Cropland	1.8	0.59	0.25	2.58×10^6	1.54
Chestnut	35.93°N, 84.33°W	Forest	5.4	0.93	0.19	2.06×10^6	1.53
Missouri	38.74°N, 92.20°W	Forest	5.4	0.93	0.30	2.53×10^6	1.70

[a]LAI, f_C, SM, C, and P, respectively, represent the leaf area index, vegetation cover fraction, soil moisture, soil heat capacity, and soil thermal conductivity.

quantities are the main factors controlling the sensible and latent heat fluxes. At all sites, the CS and DS data assimilation systems are applied to the vegetation growing period in 2006 (Julian days 151–240).

Following *De Vries* [1963], *Farouki* [1981], and *Bateni et al.* [2012], the soil volumetric heat capacity (C) and thermal conductivity (P) are determined based on soil texture and soil moisture. In this study, soil texture and moisture at each site are obtained from the Harmonized World Soil Database (HWSD) and in situ measurements (Table 1), respectively. For simplicity, we used the average of soil moisture measurements during the assimilation period.

Micrometeorological and forcing data including wind speed, air temperature, air relative humidity, atmospheric pressure, incoming solar radiation, and incoming longwave radiation as well as surface turbulent fluxes were collected at the six AmeriFlux stations every 30 min. These flux measurements allow us to examine the performance of the CS and DS VDA frameworks. Leaf area index (LAI) data (required only by the DS scheme) are obtained from the GLASS LAI product [*Liang et al.*, 2013; *Xiao et al.*, 2014]. This product is available on the Beijing Normal University data center for global change data processing and analysis (http://www.bnu-datacenter.com/) and the University of Maryland global land cover facility archive (http://glcf.umd.edu/). LST data are retrieved from GOES 12 using the split-window algorithm developed by *Sun et al.* [2004]. The GOES 12 LST data have a nominal spatial resolution of

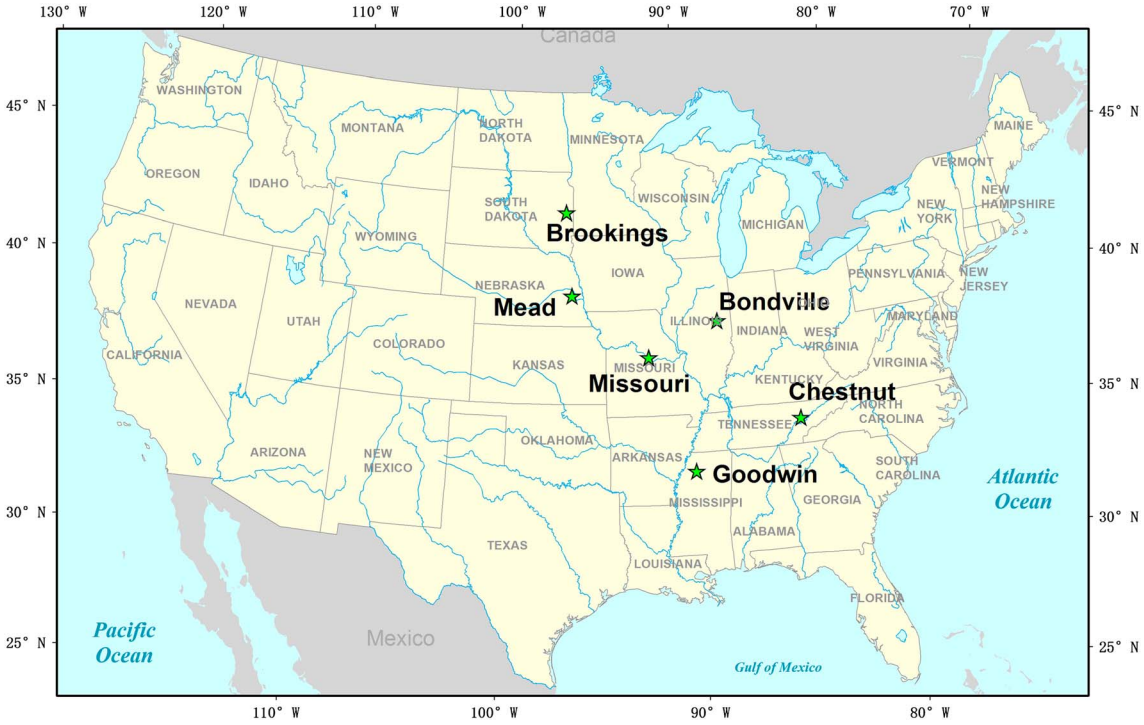

Figure 1. Locations of the six study sites.

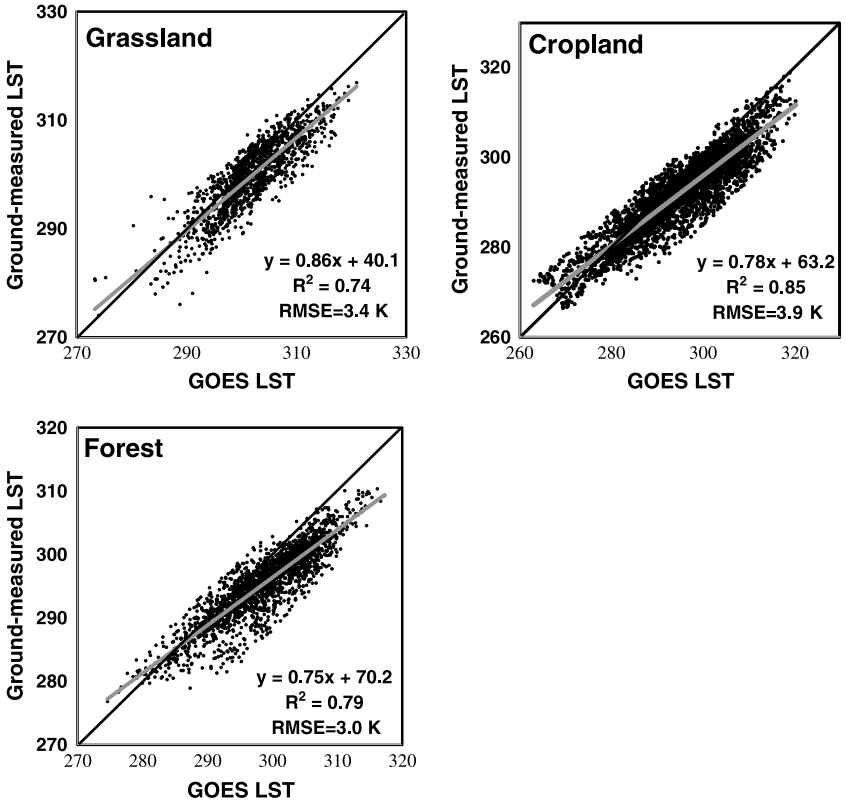

Figure 2. Comparison between the GOES LST data and ground-measured LST in sites with grassland (Brookings and Goodwin), cropland (Bondville and Mead), and forest (Chestnut and Missouri) vegetation covers.

4 km × 4 km at nadir and a revisit frequency of 30 min. The high revisit frequency of GOES LST data allows us to build the diurnal cycle of LST, which significantly advances the viability of VDA. LST observations in cloudy days are eliminated using solar radiation measurements.

The six AmeriFlux sites are classified according to their vegetation types: Brookings and Goodwin sites (grassland), Bondville and Mead sites (cropland), and Chestnut and Missouri sites (forest). The GOES LSTs are validated with ground measurements for each vegetation type during daytime hours (Figure 2). In this study, the GOES LSTs are validated only during daytime hours because the VDA system assimilates remotely sensed LSTs only in the assimilation window (i.e., 09:00–16:00 LT). As shown in Figure 2, the GOES LST data and ground measurements are highly correlated with the determination coefficient (R^2) of 0.74, 0.85, and 0.79 for grassland, cropland, and forest, respectively. For low LST values (cooler than approximately 295 K), the GOES LSTs are in good agreement with the ground measurements with the scatter mainly falling around the 1:1 line. However, for higher temperature values (warmer than approximately 295 K), the GOES LST becomes consistently larger than the ground measurements. In this study, the GOES LST data are calibrated against the measured values using the regression-based equations $y = 0.86x + 40.1$ (for grassland), $y = 0.78x + 63.2$ (for cropland), and $y = 0.75x + 70.2$ (for forest) (see Figure 2). With this calibration, the root-mean-square error (RMSE) values between the GOES and the ground-based LSTs are 3.4 K, 3.9 K, and 3.0 K, for grassland, cropland, and forest, respectively.

The relatively large scatter/offset between the GOES LST data and in situ measurements is not necessarily indicative of the poor performance of *Sun et al.*'s [2004] algorithm. As stated by *Wan et al.* [2002] and *Li et al.* [2014], it is difficult to validate the daytime LST product with ground-based LST measurements alone because of the high spatial variability in the in situ LST measurements. This means that GOES LST data usually have a large discrepancy versus in situ measurements. Although the GOES LST data have a relatively high offset, their R^2 is high which means that the GOES LST have significant correlation with ground measurements and thus can be corrected with the in situ LST observations (as done in this study).

Table 2. Neutral Bulk Heat Transfer Coefficient (C_{HN}) Estimates From the CS and DS Models[a]

	Day of Year	Brookings	Goodwin	Bondville	Mead	Chestnut	Missouri
CS	151–180	1.0×10^{-2}	1.1×10^{-2}	0.6×10^{-2}	1.7×10^{-2}	8.7×10^{-2}	5.7×10^{-2}
	181–210	1.0×10^{-2}	1.5×10^{-2}	1.3×10^{-2}	1.9×10^{-2}	10.0×10^{-2}	8.7×10^{-2}
	211–240	1.4×10^{-2}	1.5×10^{-2}	1.1×10^{-2}	2.1×10^{-2}	8.9×10^{-2}	10.9×10^{-2}
DS	151–180	1.3×10^{-2}	1.3×10^{-2}	1.1×10^{-2}	2.3×10^{-2}	8.9×10^{-2}	6.1×10^{-2}
	181–210	1.6×10^{-2}	1.5×10^{-2}	1.5×10^{-2}	2.0×10^{-2}	11.5×10^{-2}	9.8×10^{-2}
	211–240	1.8×10^{-2}	1.6×10^{-2}	1.3×10^{-2}	2.2×10^{-2}	7.9×10^{-2}	11.1×10^{-2}
LAI	151–180	1.2	1.7	1.5	1.4	5.0	5.3
	181–210	1.7	2.0	4.0	2.0	5.8	5.6
	211–240	2.0	1.6	2.5	2.0	5.4	5.4

[a]LAI represents the leaf area index.

4. Results and Discussions

4.1. Neutral Heat Transfer Coefficient and Evaporative Fraction

As mentioned in section 2, C_{HN} and EF are the two key unknown parameters in the CS model, and C_{HN}, EF_S, and EF_C constitute the three unknown parameters in the DS model. C_{HN} and EF are estimated, respectively, on monthly and daily time scales. In the VDA framework, the accuracy of turbulent heat flux estimates mainly depends on the robust retrieval of these unknown parameters.

The estimated C_{HN} values from the CS and DS schemes for the six experimental sites are shown in Table 2. C_{HN} estimates from the CS and DS models have generally the same order of magnitude and are comparable with each other over different assimilation periods. However, in most cases, the DS C_{HN} values are slightly larger than those of the CS model. The discrepancy between C_{HN} estimates from the CS and DS schemes is due to the difference in the structure of the CS and DS schemes. To understand this distinction better, the C_{HN} estimates from the CS, $(C_{HN})_{CS}$ and DS, $(C_{HN})_{DS}$, schemes are related using equations (4) and (8a):

$$(C_{HN})_{DS} = (C_{HN})_{CS}\frac{T - T_A}{T_W - T_A} \tag{15}$$

The land surface temperature (T) is usually larger than the air temperature within the canopy (T_W) during the assimilation window (i.e., $T > T_W$). Subtracting T_A from both sides of the inequality leads to $(T - T_A) > (T_W - T_A)$. Thus, the C_{HN} estimates from the DS scheme should typically be higher than those from the CS scheme (see Table 2).

LAI values over different periods are listed in Table 2 to explore the relationship between C_{HN} estimates and vegetation phenology. As shown, at each site, the C_{HN} estimates generally increase with LAI values. Remarkably, the C_{HN} estimates from both schemes are higher at sites with larger LAI values (Chestnut and Missouri) (Tables 1 and 2), implying that the VDA system can robustly retrieve C_{HN} from sequences of LST observations. This is particularly interesting because no information on vegetation phenology is used in the CS model. Yet its C_{HN} estimates are larger at sites with denser canopies.

Figure 3 shows the time series of the evaporative fraction (EF) values estimated from the CS and DS schemes. For comparison, EF observations are also shown on the same figure. The estimated EF values from the CS and DS models agree well with the observations in terms of both magnitude and day-to-day dynamics. Additionally, the DS model yields EF values closer to observations than does the CS model. Oscillations in the estimated EF values are consistent with land surface wetting and drying events. EF values increase sharply when precipitation happens and reduce in drydown periods even though no soil moisture or precipitation data are used in the model. For example, during the drydown period at the Brookings (Julian day 171 to 191), Goodwin (Julian day 191 to 211), and Missouri (Julian day 191 to 221) sites, EF estimates decrease significantly.

4.2. Sensible and Latent Heat Fluxes

Figure 4 compares the half hourly turbulent heat flux estimates from the CS and DS models with the corresponding measurements at the Brookings, Goodwin, Bondville, Mead, Chestnut, and Missouri sites, respectively. This figure allows us to evaluate the performance of the CS and DS models in different hydrological and vegetative conditions. As shown, the sensible and latent heat fluxes retrieved from both

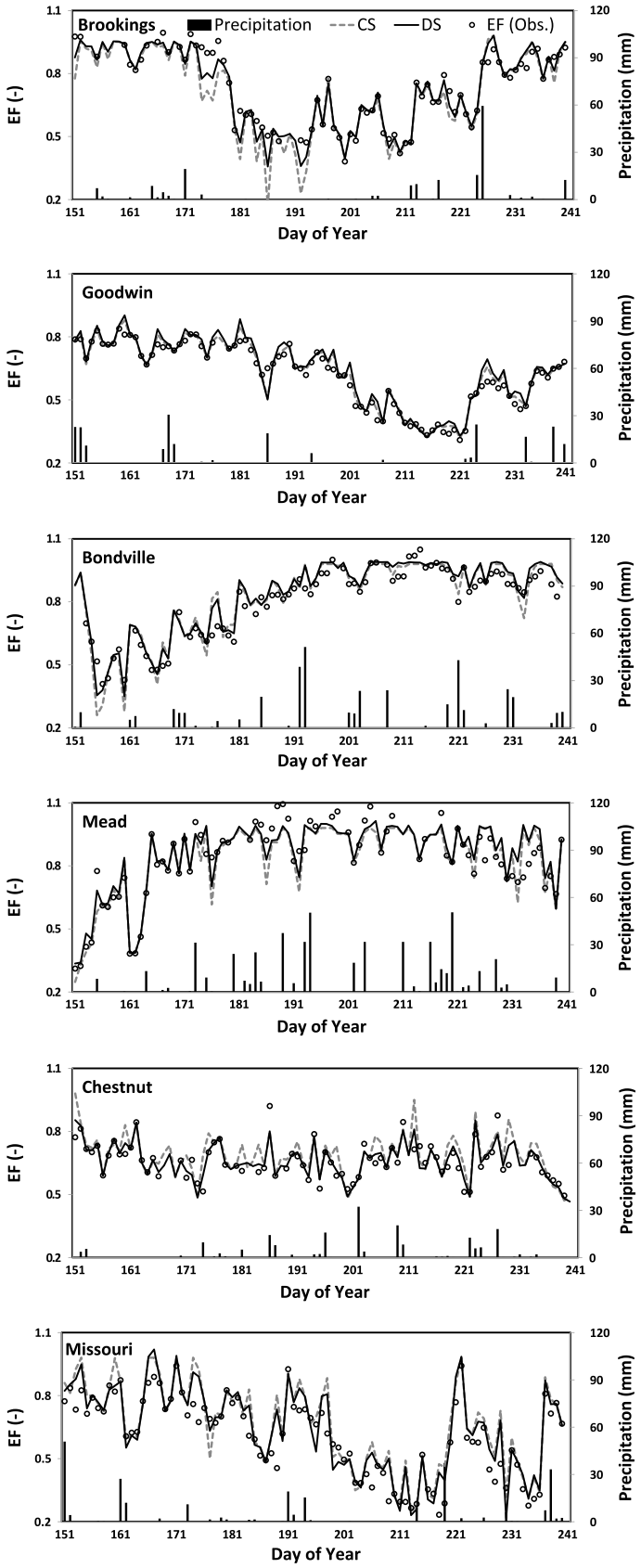

Figure 3. Time series of evaporative fraction (EF) estimates from the CS and DS models.

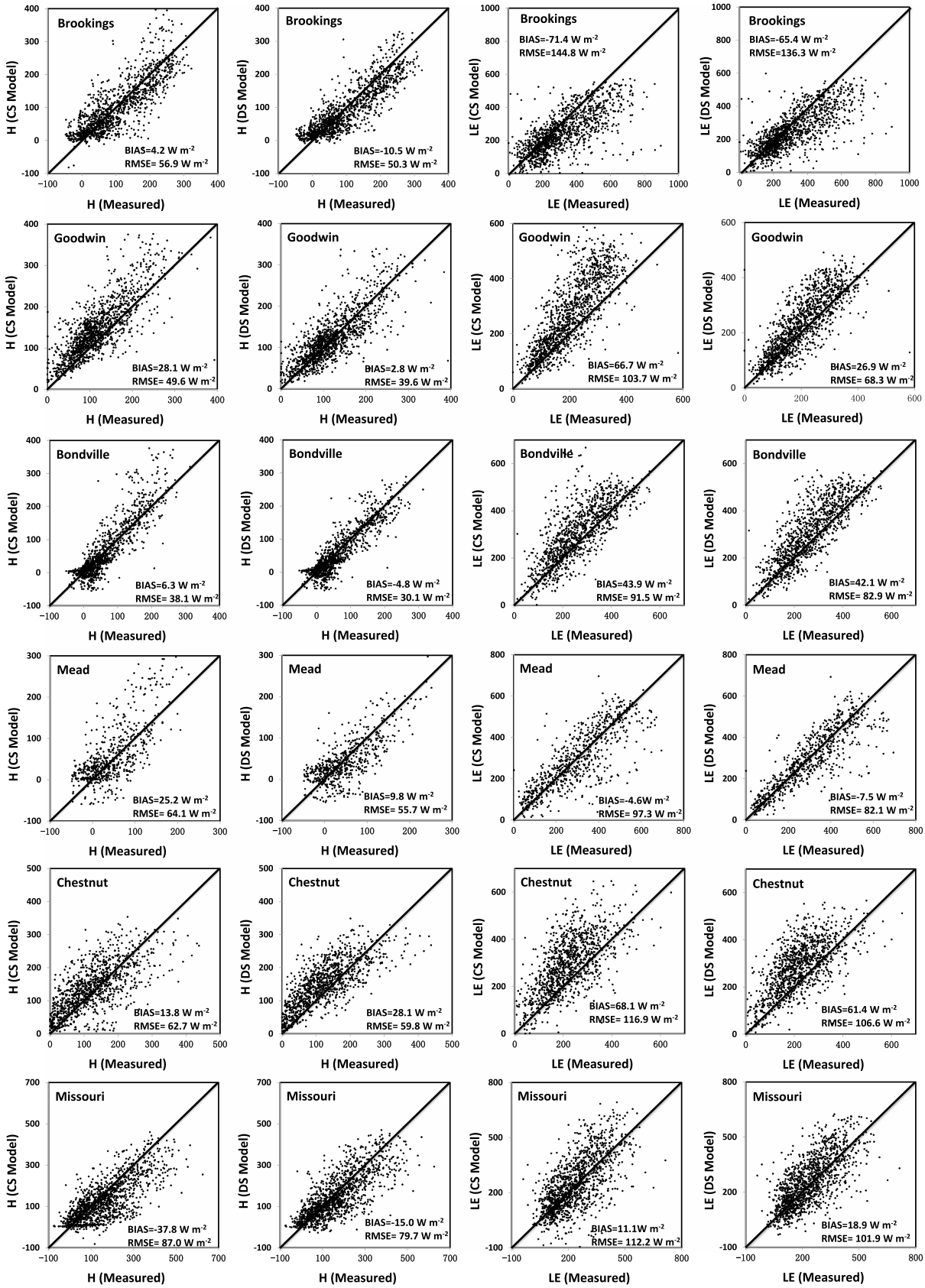

Figure 4. Scatterplots between modeled (CS and DS) and measured (EC data) sensible and latent heat fluxes (*H* and *LE*) in the six sites for Julian days 151–240 in 2006.

Table 3. The Percentage Relative Difference of Turbulent Heat Flux Estimates From the CS and DS Schemes[a]

	Day of Year	Brookings	Goodwin	Bondville	Mead	Chestnut	Missouri
P_H (%)	151–180	−20.4	−23.7	−14.3	−28.4	6.3	9.6
	181–210	−5.2	−15.9	−11.5	−24.5	9.7	14.4
	211–240	−7.7	−15.1	−22.5	−21.1	14.6	14.2
	151–240	−11.1	−18.2	−16.1	−24.7	10.2	12.7
P_{LE} (%)	151–180	3.7	18.7	10.7	11.3	−5.2	−3.1
	181–210	7.7	11.4	0.5	3.5	−2.2	−4.3
	211–240	1.4	12.8	4.6	3.9	−1.1	−2.4
	151–240	4.2	14.3	5.3	6.2	−2.8	−3.3
f_C	151–180	0.45	0.57	0.53	0.50	0.92	0.93
	181–210	0.57	0.63	0.86	0.63	0.94	0.94
	211–240	0.63	0.55	0.71	0.63	0.93	0.93
	151–240	0.55	0.59	0.74	0.59	0.93	0.93

[a] $P_H(\%) = (H(_{DS}) - H(_{CS}))/H(_{CS}) \times 100$ and $P_{LE}(\%) = (LE(_{DS}) - LE(_{CS}))/LE(_{CS}) \times 100$. $H(_{CS})$ and $H(_{DS})$ represent the sensible heat flux estimates from the CS and DS schemes, $LE(_{CS})$ and $LE(_{DS})$ denote the latent heat flux estimates from the CS and DS schemes, and f_C means vegetation cover fraction.

models are in good agreement with the observations and mainly fall around the 1:1 line. Additionally, the DS scheme performs better than the CS scheme. This is because the DS model can represent the physics of the problems more robustly. The misfits between the model estimates and observations are mainly due to the physical assumptions (constant soil thermal conductivity (P) and heat capacity (C); constant daily EF, EF_C, and EF_S; and constant monthly C_{HN}) in the CS and DS models. Over the Goodwin and Chestnut sites, both the CS and DS schemes tend to overestimate the latent heat flux when it is larger than 200 W m^{-2}. This may be due to the undermeasurement of sensible and latent heat fluxes by the eddy covariance (EC) technique, i.e., the so-called "energy imbalance" problem. The energy balance ratio (EBR = $(H + LE)/(R_N - G)$) is 0.78 and 0.75 at the Goodwin and Chestnut sites, respectively, implying that the EC method underestimates the latent heat flux. This leads to a bias greater than 60 W m^{-2} in the LE estimates at these two sites.

The bias and RMSE of the turbulent heat flux estimates at the six experimental sites are shown in Figure 4 as well. For sensible heat flux, the six-site-averaged bias (RMSE) from the CS and DS schemes are 7.5 (59.7) and 1.7 (52.5) Wm^{-2}, respectively. For latent heat flux, the six-site-averaged bias (RMSE) is 19.0 (111.1) Wm^{-2} for the CS scheme and 12.7 (96.4) Wm^{-2} for the DS scheme. The low bias and RMSE values imply that the CS and DS schemes can retrieve turbulent heat fluxes accurately.

By treating the soil and the canopy as different sources and accounting for their interaction with the overlying atmosphere in the DS model, the bias (RMSE) of the retrieved sensible and latent heat fluxes over the six experimental sites is on average 77% and 33% (12% and 13%) less than that of the CS model. Overall, the statistical metrics in Figure 4 indicate that decomposing the land surface into canopy and soil sources via the DS model improves the estimate of turbulent heat fluxes.

The discrepancies between the results of the CS and DS models are mainly due to the different model structures. The DS model treats the soil and vegetation canopy as dual sources, while the CS model treats them as combined sources. The DS model can characterize the heterogeneity of the land surface and weighs the soil and canopy fluxes via the vegetation cover fraction (f_C) (see equation (8b)), while the less elaborate CS scheme cannot. The f_C values for the six sites are listed in Table 1. As shown in Figure 4, the largest discrepancy between the CS and DS turbulent heat flux estimates occurs when f_C is approximately 0.5–0.6 (at the Goodwin and Mead sites). When f_C is about 0.5, the land surface heterogeneity is at its peak, and thus, the CS model cannot capture the physics of the underlying problem as robustly as the DS model. As a result, the maximum difference is observed between the CS and DS scheme H and LE estimates (see Table 3). As f_C increases to 0.7 (at the Bondville site), land surface patchiness decreases, and therefore, the misfit between the CS and DS model retrievals decreases (Table 3). At f_C of about 0.9 (at the Chestnut and Missouri sites), land surface patchiness reaches its minimum because the land surface is mainly composed of canopy. Consequently, the CS model can retrieve turbulent heat fluxes almost as accurately as the DS model. Turbulent heat fluxes are mainly controlled by atmospheric factors rather than land surface properties at the Brookings site since it is a wet site. Therefore, even with an f_C value of 0.55 at this site (i.e., high land surface heterogeneity),

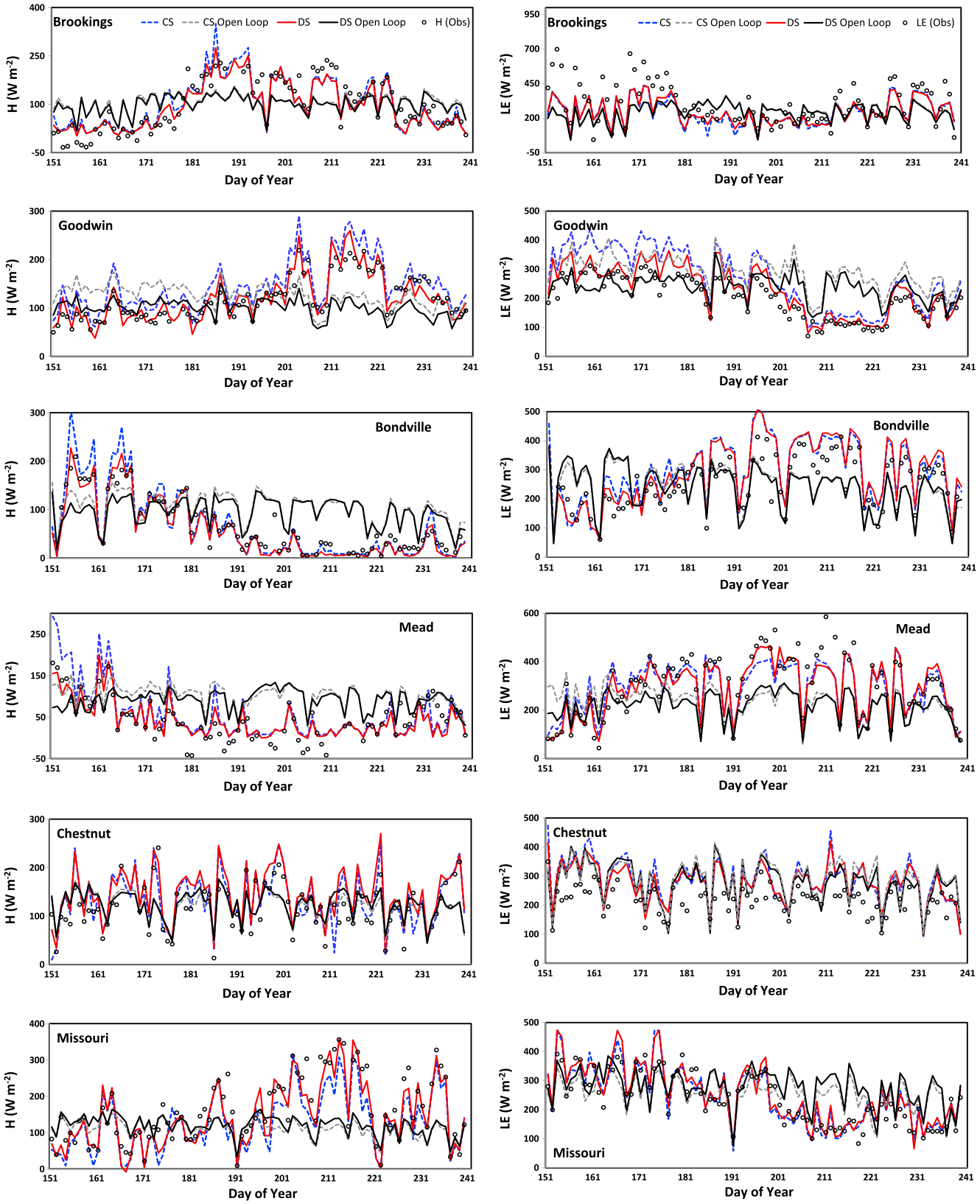

Figure 5. Time series of daytime-averaged sensible and latent heat flux (*H* and *LE*) estimates in the six experimental sites from the CS scheme with (blue dashed lines) and without (grey dashed lines) assimilation of GOES LST. Corresponding estimates from the DS scheme with (red solid lines) and without (black solid lines) assimilation of GOES LST. Observations are shown by open circles.

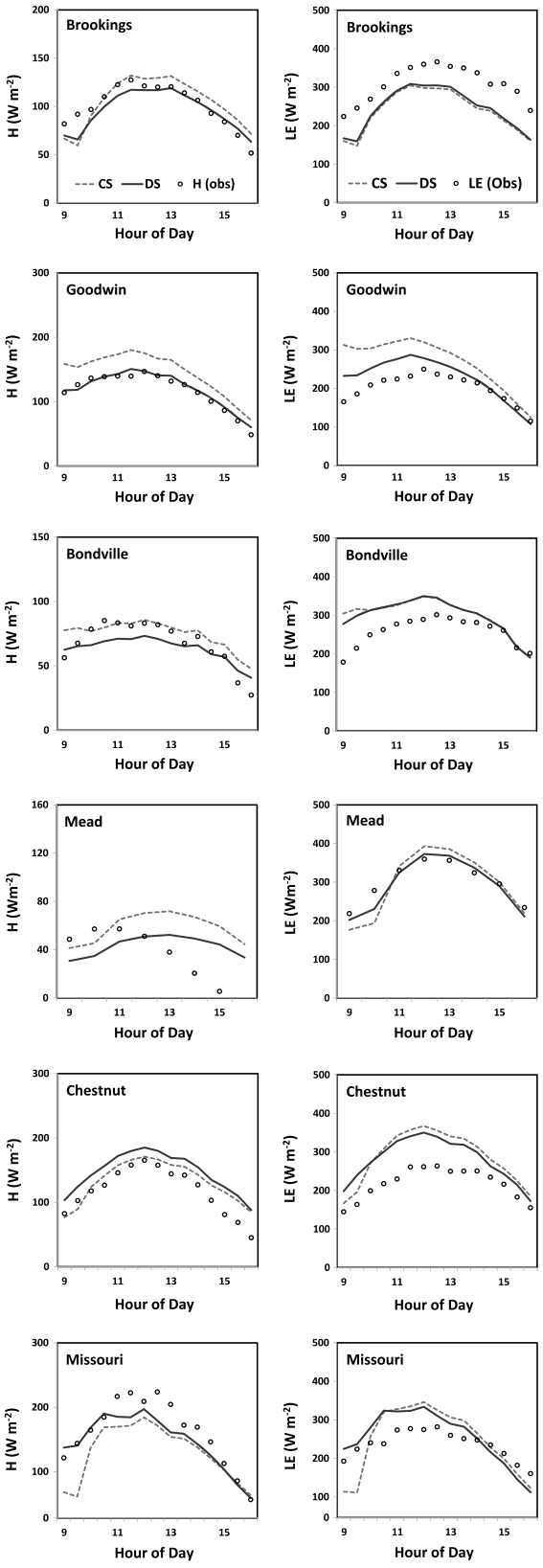

Figure 6. Mean diurnal cycle of turbulent heat flux estimates from the CS and DS models along with the observations in the six experimental sites (*H* and *LE* mean sensible and latent heat fluxes).

a small discrepancy is found between the CS and DS model estimates (Table 3). At the Bondville site, f_C illustrates a pronounced seasonal variation and increases from 0.53 (for Julian days 151–180) to 0.86 (for Julian days 181–210). As a result, the discrepancy between turbulent flux estimates from the CS and DS models is higher for Julian days 151–180 compared to Julian days 181–210 (see Table 3).

Figure 5 shows the time series of daytime-averaged (09:00–16:00 LT) estimated sensible and latent heat fluxes from the CS and DS models at the six experimental sites. Results from control experiments (i.e., without assimilation of GOES LST) and EC observations are indicated in Figure 5 as well. As indicated, the CS and DS model estimates are consistent with the observations in terms of both magnitude and day-to-day dynamics, implying that assimilating LST data from GOES can reliably partition the available energy among sensible and latent heat fluxes. However, the turbulent heat flux estimates degrade in wet periods (e.g., Julian days 151–180 at the Brookings site and Julian days 201–215 at the Mead site). At the Brookings (Mead) site, the daytime-averaged latent heat flux measurements increase to approximately 700 Wm^{-2} (600 Wm^{-2}) in the corresponding aforementioned wet periods, while the model estimates cannot reach those high values. This happens because the upper bound of EF (EF_S and EF_C) in the CS (DS) model is set to 0.97 to avoid numerical instabilities (Figure 3), while the corresponding EF observations are sometimes larger than 1.0 due to negative sensible heat flux measurements (according to equation (5), negative sensible heat flux measurements lead to EF values larger than 1.0). As indicated in Figure 5, the estimated *H* and *LE* values from the VDA models are closer to the observations than those of the control experiments. The good agreement between the estimated and observed turbulent heat fluxes illustrates that the VDA model can effectively use implicit information in the LST observations to constrain the unknowns of the CS and DS schemes. In contrast, the control experiments perform poorly since there is no constraint by the LST observations.

Figure 6 shows the mean diurnal cycle of observed and estimated turbulent heat fluxes from the CS and DS models at the six

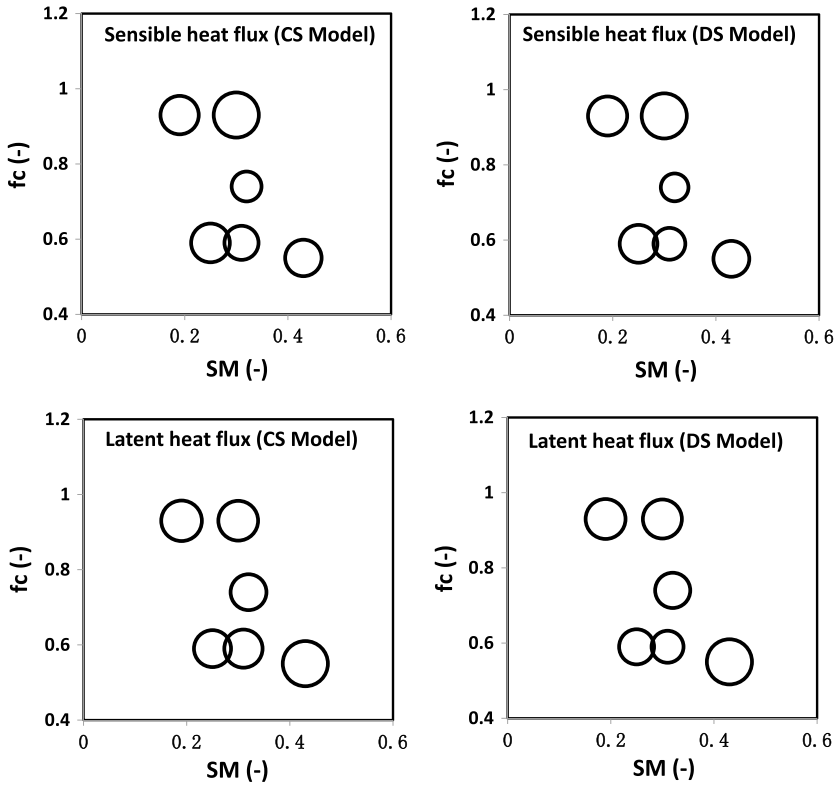

Figure 7. The relationship between the RMSE of turbulent heat flux estimates at each site and its soil moisture (SM) and vegetation cover fraction (f_C). Circle size is determined by the RMSE of flux estimates at each site (larger circles indicate higher RMSE values).

experimental sites. As indicated, the diurnal variations of retrieved turbulent heat fluxes from both models agree well with those of the observations in terms of magnitude and phase. A large discrepancy between the CS and DS model diurnal cycles is found at the Goodwin ($f_C = 0.59$) and Mead ($f_C = 0.59$) sites, which have high land surface heterogeneity. In contrast, at sites in which the land surface tends to be more homogeneous (e.g., Bondville, Chestnut, and Missouri, with f_C of 0.74, 0.93, and 0.93, respectively), the diurnal cycle retrievals from the CS and DS scheme are close. At the Chestnut site, the CS and DS models overestimate both the sensible and latent heat fluxes. This is mainly because turbulent heat flux measurements from the EC system at the Chestnut site may contain errors and suffer from the energy imbalance problem. Overall, the misfit between the observed and estimated diurnal cycles is due to a number of reasons, including the assumptions of constant daily evaporative fraction and constant monthly neutral bulk heat transfer coefficient and the use of constant soil thermal properties over the modeling period.

Figure 7 shows the relationship between RMSE of turbulent heat flux estimates at each of the six explored sites and its soil moisture and vegetation cover fraction. Each circle corresponds to one site, and its size represents the RMSE of flux estimates at the site (larger circles illustrate higher RMSE values). As indicated, the CS and DS models perform better at dry and/or sparsely vegetated sites than at wet and/or densely vegetated sites. Similarly, the results in Figure 4 indicate that the CS and DS schemes yield larger biases and RMSE values (less accurate turbulent heat fluxes) over densely vegetated/wet sites than over lightly vegetated/dry sites. For example, the bias and RMSE of turbulent heat flux estimates at the Chestnut and Missouri sites with denser vegetation cover (i.e., higher LAI value) are larger than those at the Goodwin, Bondville, and Mead sites with lower canopy cover. Additionally, at the Brookings site, which has higher soil moisture, the turbulent heat flux retrievals degrade compared to the drier Goodwin, Bondville, and Mead sites.

In another effort, *Crow and Kustas* [2005] tested only the CS VDA system with the force-restore equation as an adjoint (VDA-FR) over a range of vegetative and hydrological conditions in the southern U.S.. They found that the performance of the CS VDA-FR framework degraded over densely vegetated and/or wet sites, and suggested that additional land surface information (e.g., LAI) is required to accurately predict surface heat

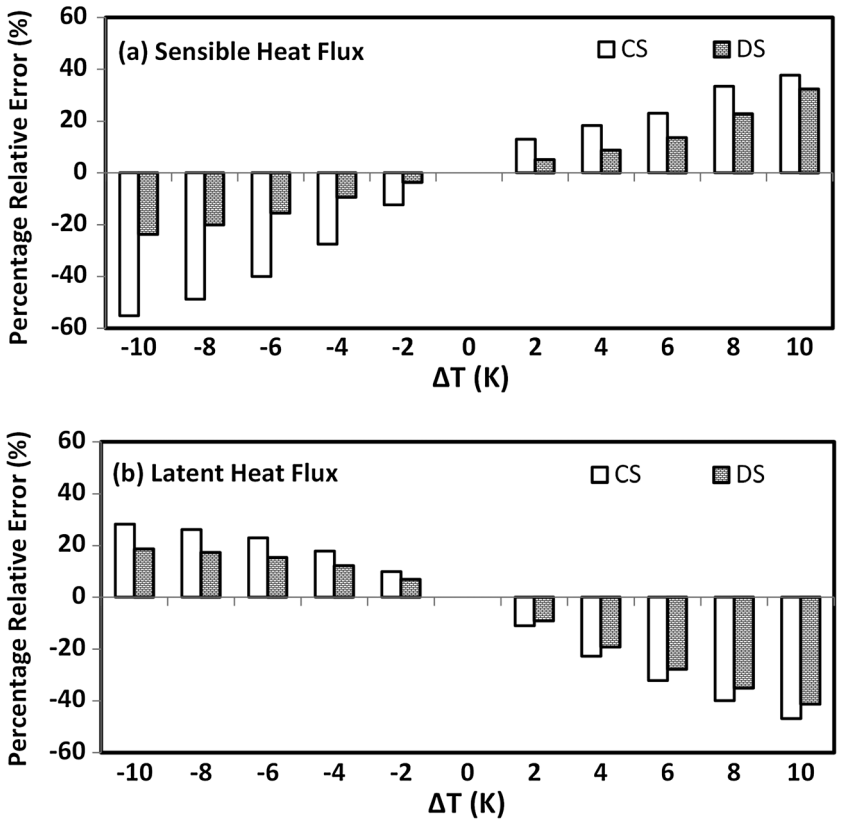

Figure 8. (a) The percentage relative error (($H_{\text{sensitivity test}} - H_{\text{original}}$)/$H_{\text{original}} \times 100$) of estimated sensible heat flux by different sensitivity tests accounting for uncertainties in LST. The original run sensible heat flux estimates (H_{original}) are obtained by the CS and DS models with the nominal LST observations at the Bondville site. (b) The same as in Figure 8a but for latent heat flux.

fluxes in densely vegetated and wet sites. In comparison to the *Crow and Kustas*' [2005] study, this work tested both the CS and DS VDA systems with the full heat diffusion equation (instead of the parsimonious force-restore equation) over six sites across the U.S.. Since even the DS scheme (that uses LAI) cannot perform robustly in densely vegetated/wet sites, it is suggested to assimilate soil moisture or rainfall observations within the VDA scheme in future studies.

5. Uncertainty Analysis

In addition to LST which lies at the heart of the surface energy balance equation and has information on the partitioning of available energy among the surface energy balance components [*Bateni and Entekhabi*, 2012a, 2012b], LAI variations (used only in the DS model) control this partitioning [*Segal et al*., 1988; *Alfieri et al*., 2009; *Bateni et al*., 2013b]. In this section, a number of sensitivity tests are performed to understand the impact of uncertainties in LST and LAI on the surface turbulent flux estimates. The main goal of sensitivity tests is to provide insights into the effect of errors in LST and LAI on the performance of VDA system. The Bondville site is selected for this purpose in this study. In the first set of tests, LST observations are varied by ±2, ±4, ±6, ±8, and ±10 K from their nominal values and are used in the CS and DS schemes to estimate turbulent heat fluxes. Figure 8 shows the sensitivity of *H* and *LE* estimates from the CS and DS schemes to uncertainties in LST. For the CS approach, increasing LST by 2, 4, 6, 8, and 10 K leads to a 13.0%, 18.3%, 23.0%, 33%, and 37.8% reductions in *H* and a 10.9%, 22.8%, 32.1%, 39.9%, and 46.9% increase in *LE*. On the other hand, decreases in LST by 2, 4, 6, 8, and 10 K causes *H* to be decreased by 12.4%, 27.5%, 40.1%, 48.8%, and 55.1% and causes *LE* to be increased by 9.9%, 17.9%, 22.9%, 26.1%, and 28.3%. As indicated in Figure 8, the estimated turbulent heat fluxes from the DS scheme are less sensitive to the uncertainties in LST (i.e., the DS model performs better than the CS model when biased LST data are assimilated). For example, *H* and *LE* estimates vary 13.6% and 27.8% as LST becomes 6 K larger than its nominal value.

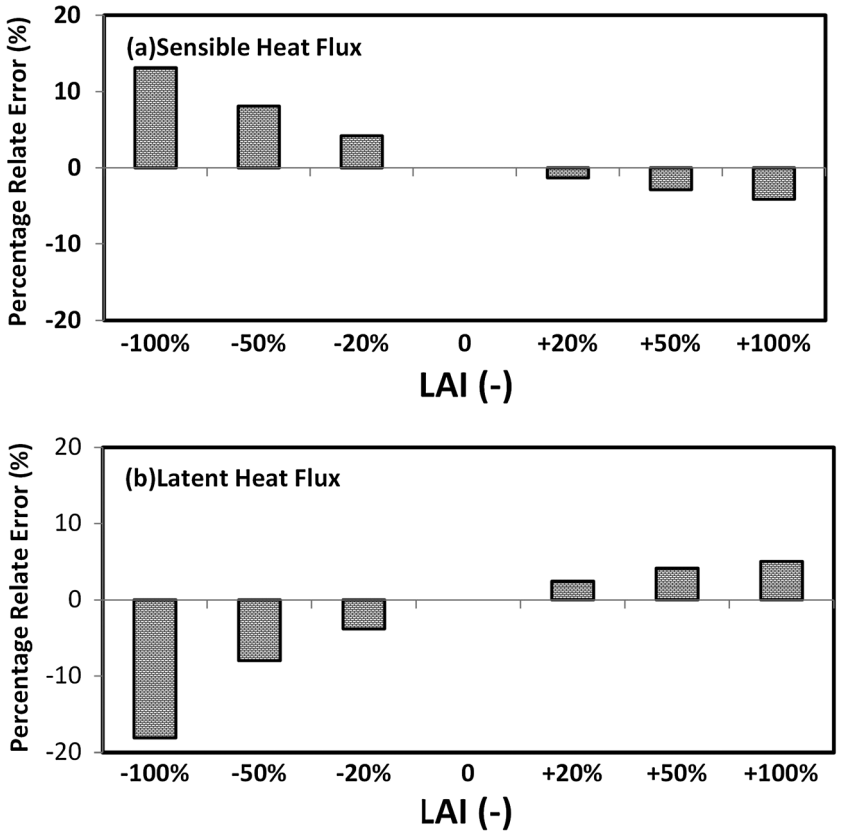

Figure 9. (a) The percentage relative error (($H_{\text{sensitivity test}} - H_{\text{original}}$)/$H_{\text{original}} \times 100$) of estimated sensible heat flux by different sensitivity tests accounting for uncertainties in leaf area index (LAI). The original run sensible heat flux estimates (H_{original}) are obtained by the CS and DS models with the nominal LAI observations at the Bondville site. (b) The same as in Figure 9a but for latent heat flux.

To assess the effect of variations in LAI on the sensible and latent heat flux estimates, the nominal LAI values are varied by ±20%, ±50%, and ±100% and are used in the DS model. Since the CS model does not use LAI, the sensitivity tests herein are performed with the DS approach only. The sensitivity of estimated sensible and latent heat fluxes to variations in LAI is indicated in Figure 9. Decreasing LAI by 20%, 50%, and 100% yields a 4.2%, 8.1%, and 13.1% increase in sensible heat flux and a 3.8%, 8.0%, and 18.1% reduction in latent heat flux. Also, the DS model tends to yield larger errors when fed with underestimated leaf area index values. Overall, all of these results clearly demonstrate that the correct specification of LST and LAI plays an important role in the accurate retrieval of turbulent heat fluxes. These findings also allow us to quantitatively characterize the effect of uncertainties in LST and LAI on the turbulent heat flux estimates.

6. Conclusions

Land surface temperature (LST) data retrieved from the Geostationary Operational Environmental Satellites (GOES) are assimilated into the combined-source (CS) and dual-source (DS) variational data assimilation (VDA) frameworks. The CS scheme does not account for the difference between soil and canopy and considers the land surface as one effective medium. In contrast, the DS scheme separates the land surface into soil and vegetation sources and accounts for the interaction of each source with the overlying atmosphere. The unknown parameters of the CS scheme are the neutral heat transfer coefficient (C_{HN}) and evaporative fraction (EF). Similarly, the unknowns of the DS scheme are C_{HN} and soil and canopy evaporative fraction (EF_S and EF_C). By minimizing the difference between LST estimates (from the heat diffusion equation) and observations (from GOES) via the utilized VDA framework, the optimal values of monthly C_{HN} and daily EF (EF_S and EF_C) are retrieved, and the surface turbulent fluxes can be estimated accordingly.

In this study, the CS and DS schemes are tested at six AmeriFlux sites, which sample a fairly wide range of hydrological and vegetative conditions. C_{HN} estimates from the CS and DS models have the same order of magnitude and are comparable over different assimilation periods. Their temporal variations are consistent with the vegetation phenology at each site. Also, C_{HN} estimates at densely vegetated sites (e.g., the Chestnut and Missouri sites) are higher than those at sites with sparse canopy cover (e.g., the Brookings, Goodwin, Bondville, and Mead sites). This is an interesting finding, specifically for the CS model, because it does not use any information on vegetation phenology. Yet variations in its C_{HN} estimates are consistent with those of LAI. The EF estimates are in agreement with the observations in terms of magnitude and day-to-day dynamics even though no rainfall or soil moisture data are used in the model. These results indicate that assimilating the sequences of GOES LST can partition the available energy between the sensible and latent heat fluxes.

For the CS VDA scheme, the six-site-averaged RMSE value is 59.7 W m^{-2} for sensible heat flux and 111.1 W m^{-2} for latent heat flux. The DS model reduces the aforementioned RMSEs by 12% and 13%, respectively, because it accounts for the interaction between soil and canopy and considers the contributions of soil and canopy to the total sensible and latent heat fluxes. The misfit between the estimated and observed turbulent heat fluxes is attributed to the assumptions made in the models (e.g., constant soil heat conductivity; constant soil thermal conductivity; daily constant EF, EF_C, and EF_S; and monthly constant C_{HN}) as well as errors in measured sensible and latent heat fluxes (the so-called energy imbalance problem).

The largest discrepancy between the CS and DS turbulent heat flux retrievals was found when f_C is about 0.5 (at the Goodwin and Mead sites). In this condition, the land surface heterogeneity reaches its maximum, and the CS model cannot characterize the physics of the problem as accurately as the DS model. With the increase of f_C to about 0.7 (at the Bondville site) or 0.9 (at the Chestnut and Missouri sites) (i.e., decrease of land surface patchiness), the difference in turbulent heat flux estimates from the CS and DS schemes is reduced because the CS model can represent the land-atmosphere interaction almost as well as the DS model.

The performance of the CS and DS schemes is better at dry/sparsely vegetated sites compared to wet/densely vegetated sites. The first reason is that EF is limited to an upper bound of 0.97 in the data assimilation system to avoid numerical instabilities, although in wet/densely vegetated conditions, EF can exceed 1. The second reason is that in wet conditions, *LE* is mainly controlled by atmospheric factors rather than land surface properties.

The sensitivity of turbulent heat flux predictions to uncertainty in land surface temperature and leaf area index (as two key factors affecting *H* and *LE*) is quantitatively characterized. It is found that the CS model is more sensitive to uncertainties in land surface temperatures compared to the DS model. Also, the DS model tends to yield larger errors when fed with underestimated leaf area index values.

This study estimates the turbulent heat fluxes via assimilation of sequences of LST observations within a VDA framework. The heat diffusion equation, which generates LST, is utilized as the dynamic model. The water balance model is not used in the CS and DS VDA systems. Therefore, the key advantage of these schemes is that they do not require extra input variables such as soil moisture or precipitation. However, these VDA schemes cannot work well over densely vegetated and/or wet conditions as shown in this study. Future studies should focus on introducing the soil wetness model forced by rainfall data or the water balance model constrained by soil moisture observations to improve the performance of the VDA schemes in wet conditions.

In this work, performances of the CS and DS VDA systems are compared extensively over several sites with different hydrological conditions. Upcoming efforts should concentrate on comparing the results of VDA approach with those of other methods such as triangle, maximum entropy, and NASA Land Information System.

Acknowledgments

The authors thank three anonymous reviewers for their helpful comments and suggestions that have significantly improved this article. We thank NOAA CLASS for providing the GOES data used in this study. The eddy covariance and meteorology data were downloaded freely via AmeriFlux networks (http://public.ornl.gov/ameriflux). The soil texture data are obtained from the Harmonized World Soil Database (HWSD). Leaf area index (LAI) data are available on the Beijing Normal University data center (http://www.bnu-datacenter.com/) and the University of Maryland global land cover facility archive (http://glcf.umd.edu/). This work was funded by the High-Tech Research and Development Program of China (2013AA122800), the National Natural Science Foundation of China (41201330), the Water Resource Research Center at the University of Hawaii at Manoa, the Fundamental Research Funds for the Central Universities (2012LYB37), and the Special Foundation for Free Exploration of State Key Laboratory of Remote Sensing Science (grant 13ZY-06).

References

Alfieri, J. G., X. Xiao, D. Niyogi, R. A. Pielke, F. Chen, and M. A. LeMone (2009), Satellite-based modeling of transpiration from the grasslands in southern great plains, USA, *Global Planet. Change*, *67*(1–2), 78–86.

Anderson, M. C., J. M. Norman, G. R. Diak, W. P. Kustas, and J. R. Mecikalski (1997), A two-source time-integrated model for estimating surface fluxes using thermal infrared remote sensing, *Remote Sens. Environ.*, *60*(2), 195–216, doi:10.1016/S0034-4257(96)00215-5.

Bastiaanssen, W. G. M., M. Menenti, R. A. Feddes, and A. A. M. Holtslag (1998a), A remote sensing surface energy balance algorithm for land (SEBAL): 1. Formulation, *J. Hydrol.*, *212-213*, 198–212, doi:10.1016/S0022-1694(98)00253-4.

Bastiaanssen, W. G. M., H. Pelgrum, J. Wang, Y. Ma, J. F. Moreno, G. J. Roerink, and T. van der Wal (1998b), A remote sensing surface energy balance algorithm for land (SEBAL): 2. Validation, *J. Hydrol.*, *212-213*, 213–229, doi:10.1016/S0022-1694(98)00254-6.

Bateni, S. M., and D. Entekhabi (2012a), Relative efficiency of land surface energy balance components, *Water Resour. Res.*, *48*, W04510, doi:10.1029/2011WR011357.

Bateni, S. M., and D. Entekhabi (2012b), Surface heat flux estimation with the ensemble Kalman smoother: Joint estimation of state and parameters, *Water Resour. Res.*, *48*, W08521, doi:10.1029/2011WR011542.
Bateni, S. M., and S. Liang (2012), Estimating surface energy fluxes using a dual-source data assimilation approach adjoined to the heat diffusion equation, *J. Geophys. Res.*, *117*, D17118, doi:10.1029/2012JD017618.
Bateni, S. M., D. S. Jeng, and S. M. M. Naeini (2012), Estimating soil thermal properties from sequences of land surface temperature using hybrid Genetic Algorithm-Finite Difference method, *Eng. Appl. Artif. Intell.*, *25*(7), 1425–1436.
Bateni, S. M., D. Entekhabi, and D. S. Jeng (2013a), Variational assimilation of land surface temperature and the estimation of surface energy balance components, *J. Hydrol.*, *481*, 143–156, doi:10.1016/j.jhydrol.2012.12.039.
Bateni, S. M., D. Entekhabi, and F. Castelli (2013b), Mapping evaporation and estimation of surface control of evaporation using remotely sensed land surface temperature from a constellation of satellites, *Water Resour. Res.*, *49*, 950–968, doi:10.1002/wrcr.20071.
Bennett, A. F. (2002), *Inverse Modeling of the Ocean and Atmosphere*, Cambridge Univ. Press, U. K.
Boni, G., D. Entekhabi, and F. Castelli (2001), Land data assimilation with satellite measurements for the estimation of surface energy balance components and surface control on evaporation, *Water Resour. Res.*, *37*, 1713–1722, doi:10.1029/2001WR900020.
Caparrini, F., F. Castelli, and D. Entekhabi (2003), Mapping of landatmosphere heat fluxes and surface parameters with remote sensing data, *Boundary Layer Meteorol.*, *107*(3), 605–633.
Caparrini, F., F. Castelli, and D. Entekhabi (2004a), Estimation of surface turbulent fluxes through assimilation of radiometric surface temperature sequences, *J. Hydrometeorol.*, *5*, 145–159.
Caparrini, F., F. Castelli, and D. Entekhabi (2004b), Variational estimation of soil and vegetation turbulent transfer and heat flux parameters from sequences of multisensor imagery, *Water Resour. Res.*, *40*, W12515, doi:10.1029/2004WR003358.
Castelli, F., D. Entekhabi, and E. Caporali (1999), Estimation of surface heat transfer and an index of soil moisture using adjoint-state surface energy balance, *Water Resour. Res.*, *35*, 3115–3126, doi:10.1029/1999WR900140.
Crow, W. T., and W. P. Kustas (2005), Utility of assimilating surface radiometric temperature observations for evaporative fraction and heat transfer coefficient retrieval, *Boundary Layer Meteorol.*, *115*(1), 105–130, doi:10.1007/s10546-004-2121-0.
de Vries, D. A. (1963), Thermal properties of soils, in *Physics of Plant Environment*, edited by W. R. van Wijk, pp. 210–235, North-Holland, New York.
Farouki, O. T. (1981), The thermal properties of soils in cold regions, *Cold Reg. Sci. Technol.*, *5*, 67–75.
Gentine, P., D. Entekhabi, and A. Chehbouni (2007), Analysis of evaporative fraction diurnal behavior, *Agric. For. Meteorol.*, *143*(1–2), 13–29.
Hu, Z., and S. Islam (1995), Prediction of ground temperature and soil moisture content by the force-restore method, *Water Resour. Res.*, *31*, 2531–2539, doi:10.1029/95WR01650.
Jensen, N. O., and P. Hummelshøj (1995), Derivation of canopy resistance for water vapour fluxes over a spruce forest, using a new technique for the viscous sublayer resistance, *Agric. For. Meteorol.*, *73*, 339–352.
Jia, L., G. Xi, S. Liu, C. Huang, Y. Yan, and G. Liu (2009), Regional estimation of daily to annual regional evapotranspiration with MODIS data in the Yellow River Delta wetland, *Hydrol. Earth Syst. Sci.*, *13*, 1775–1787.
Jiang, L., and S. Islam (2001), Estimation of surface evaporation map over Southern Great Plain using remote sensing data, *Water Resour. Res.*, *37*, 329–340, doi:10.1029/2000WR900255.
Jiang, L., and S. Islam (2003), An intercomparison of regional latent heat flux estimation using remote sensing data, *Int. J. Remote Sens.*, *24*(11), 2221–2236.
Kustas, W. P., K. S. Humes, J. M. Norman, and M. S. Moran (1996), Single and dual-source modeling of surface energy fluxes with radiometric surface temperature, *J. Appl. Meteorol.*, *35*(1), 110–121.
Li, H., D. L. Sun, Y. Y. Yu, H. Y. Wang, Y. L. Liu, Q. H. Liu, Y. M. Du, H. S. Wang, and B. A. Cao (2014), Evaluation of the VIIRS and MODIS LST products in an arid area of Northwest China, *Remote Sens. Environ.*, *142*, 111–121.
Liang, S., et al. (2013), A long-term Global Land Surface Satellite (GLASS) dataset for environmental studies, *Int. J. Digital Earth*, *6*(1), 5–33.
Liu, S. M., G. Hu, L. Lu, and D. F. Mao (2007a), Estimation of regional evapotranspiration by TM/ETM+ data over heterogeneous surfaces, *Photogramm. Eng. Remote Sens.*, *73*, 1169–1178.
Liu, S. M., L. Lu, D. Mao, and L. Jia (2007b), Evaluating parameterizations of aerodynamic resistance to heat transfer using field measurements, *Hydrol. Earth Syst. Sci.*, *11*, 769–783.
Liu, S. M., Z. W. Xu, W. Z. Wang, Z. Z. Jia, M. J. Zhu, J. Bai, and J. M. Wang (2011), A comparison of eddy-covariance and large aperture scintillometer measurements with respect to the energy balance closure problem, *Hydrol. Earth Syst. Sci.*, *15*, 1291–1306.
Liu, S. M., Z. W. Xu, Z. L. Zhu, Z. Z. Jia, and M. J. Zhu (2013), Measurements of evapotranspiration from eddy-covariance systems and large aperture scintillometers in the Hai River Basin, China, *J. Hydrol.*, *487*, 24–38.
Ma, W., M. Hafeez, U. Rabbani, H. Ishikawa, and Y. Ma (2012), Retrieved actual ET using SEBS model from Landsat-5 TM data for irrigation area of Australia, *Atmos. Environ.*, *59*, 408–414.
McNaughton, K. G., and B. J. J. M. Van den Hurk (1995), A Lagrangian revision of the resistors in the two-layer model for calculating the energy budget of a plant canopy, *Boundary Layer Meteorol.*, *74*, 261–288.
Nishida, K., R. R. Nemani, J. M. Glassy, and S. W. Running (2003), Development of an evapotranspiration Index from Aqua/MODIS for monitoring surface moisture status, *IEEE Trans. Geosci. Remote Sens.*, *41*(2), 493–500.
Norman, J. M., W. P. Kustas, and K. Humes (1995), A two-source approach for estimation of soil and vegetation energy fluxes from observations of directional radiometric surface temperature, *Agric. For. Meteorol.*, *77*(3), 263–293.
Qin, J., S. Liang, R. Liu, H. Zhang, and B. Hu (2007), A weak-constraintbased data assimilation scheme for estimating surface turbulent fluxes, *IEEE Geosci. Remote Sens. Lett.*, *4*(4), 649–653, doi:10.1109/LGRS.2007.904004.
Qualls, R. J., and W. Brutsaert (1996), Effect of vegetation density on the parameterization of scalar roughness to estimate spatially distributed sensible heat fluxes, *Water Resour. Res.*, *32*, 645–652, doi:10.1029/95WR03097.
Segal, M., R. Avissar, M. C. McCumber, and R. A. Pielke (1988), Evaluation of vegetation effects on the generation and modification of meso-scale circulations, *J. Atmos. Sci.*, *45*(16), 2268–2293.
Sini, F., G. Boni, F. Caparrini, and D. Entekhabi (2008), Estimation of large-scale evaporation fields based on assimilation of remotely sensed land temperature, *Water Resour. Res.*, *44*, W06410, doi:10.1029/2006WR005574.
Su, Z. (2002), The Surface Energy Balance System (SEBS) for estimation of turbulent heat fluxes, *Hydrol. Earth Syst. Sci.*, *6*, 85–100, doi:10.5194/hess-6-85-2002.
Sun, D., R. T. Pinker, and J. B. Rasara (2004), Land surface temperature estimation from the next generation of Geostationary Operationary Environmental Satellites: GOES M-Q, *J. Appl. Meteorol.*, *43*, 363–372.
Sun, L., S. Liang, W. Yuan, and Z. Chen (2013), Improving a Penman-Monteith evapotranspiration model by incorporating soil moisture control on soil evaporation in semiarid areas, *Int. J. Digital Earth*, *6*(1), 134–156.

Tang, R., Z. L. Li, and B. Tang (2010), An application of the Ts-VI triangle method with enhanced edges determination for evapotranspiration estimation from MODIS data in arid and semi-arid regions: Implementation and validation, *Remote Sens. Environ.*, *114*, 540–551.

Wan, Z. M., Y. Zhang, Q. Zhang, and Z. L. Li (2002), Validation of the land surface temperature products retrieved from Terra Moderate Resolution Imaging Spectroradiometer data, *Remote Sens. Environ.*, *83*, 163–180.

Wang, K., Z. Li, and M. Cribb (2006), Estimating of evaporative fraction from a combination of day and night land surface temperature and NDVI: A new method to determine the Priestley-Taylor parameter, *Remote Sens. Environ.*, *102*(3-4), 293–305.

Xiao, Z. Q., S. Liang, J. D. Wang, P. Chen, X. J. Yin, L. Q. Zhang, and J. L. Song (2014), Use of general regression neural networks for generating the GLASS leaf area index product from time-series MODIS surface reflectance, *IEEE Trans. Geosci. Remote Sens.*, *52*, 209–223.

Xu, T. R., S. Liang, and S. Liu (2011), Estimating turbulent fluxes through assimilation of geostationary operational environmental satellites data using ensemble Kalman filter, *J. Geophys. Res.*, *116*, D09109, doi:10.1029/2010JD015150.

Zhang, Q., S. Wang, M. Barlage, W. Tian, and R. Huang (2010), The characteristics of the sensible heat and momentum transfer coefficients over the Gobi in Northwest China, *Int. J. Clim.*, *31*(4), 621–629, doi:10.1002/joc.2071.